Osteoarthritis and Cartilage 34 (2026) 1314–1324

Osteoarthritis and Cartilage

OARSI OSTEOARTHRITIS RESEARCH SOCIETY INTERNATIONAL

The zone of calcified cartilage: A human explant culture model and a proof-of-concept transcriptomic study of 3D laser-cut interface tissue

Andrea Schwab [a b c *], Judith Veldman [a], Nicole Kops [a], Wilfred F.J. van IJcken [d], Heiko Richter [e], Merve Sinram [e], Xander den Dekker [d], Kayleigh Hiscock [d], Jessica Bertrand [b], Eric Farrell [c], Gerjo JVM van Osch [a f g]

[a] Department of Orthopaedics and Sports Medicine, Erasmus MC, University Medical Center Rotterdam, Rotterdam, the Netherlands
[b] Experimental Orthopedics, Otto-von-Guericke-University Magdeburg, Medical Faculty, University Orthopaedic Clinic, Magdeburg, Germany
[c] Department of Oral and Maxillofacial Surgery, Erasmus MC, University Medical Center Rotterdam, Rotterdam, the Netherlands
[d] Center for Biomics, Erasmus MC, University Medical Center Rotterdam, Rotterdam, the Netherlands
[e] LLS ROWIAK LaserLabSolutions GmbH, Hannover, Germany
[f] Department of Otorhinolaryngology, Head and Neck Surgery, Erasmus MC, University Medical Center Rotterdam, Rotterdam, the Netherlands
[g] Department of Biomechanical Engineering, Faculty of Mechanical Engineering, Delft University of Technology, Delft, the Netherlands

ARTICLE INFO

Article history:
Received 10 November 2025
Accepted 8 May 2026

Keywords:
Osteoarthritis
Chondrocytes
RNA-Seq
Model
In Vitro Techniques
Articular Cartilage
Cartilage-bone interface

ABSTRACT

Objective: The cartilage-bone interface, including the zone of calcified cartilage (ZCC), is a thin layer of calcified tissue with a low cell number, thus making it technically challenging to study. The aim of this study was to develop methods to selectively study the ZCC for gene expression analysis and transcriptomic studies.
Design: We set-up a method to isolate ZCC explants comprising the ZCC and a thin layer of subchondral bone from human osteochondral tissue (n=4 patients) for tissue culture. The cellular response to a pro-inflammatory cytokine cocktail or TGF-ß1 (72 h) was compared to unstimulated explants. Full-thickness non-calcified cartilage (NCC) was used as control group. Next, we have set-up an optical coherence tomography (OCT)-guided 3D-laser microtomy to isolate the calcified ZCC and used FLASH-seq technology (n=4 patients) to characterize the cells in the ZCC compared to donor-matched deep zone of non-calcified cartilage (dNCC).
Results: The culture model revealed metabolically active cells in ZCC explants that responded to inflammatory cytokines and to TGF-ß1. The responses were clearly different from the responses of NCC. With 3D-laser microtomy we isolated sufficient RNA from fresh human ZCC. ZCC had similar expression of cartilage-associated genes, lower expression of angiogenesis-related genes, and higher expression of *SOST* compared to dNCC.
Conclusion: The ZCC explant model holds promise to decipher the role of the cartilage-bone interface in disease progression. OCT-guided 3D-laser microtomy and FLASH-seq are innovative technologies overcoming the limitation of standard approaches to phenotypically characterize chondrocytes in the thin ZCC layer and in other calcified tissues.

Introduction

Tissue interfaces integrate two types of tissues resulting in gradients in mechanical properties, microstructure and matrix composition [1]. Specialized cells residing in interface tissues have a key role in controlling tissue homeostasis in health and in disease. The zone of calcified cartilage (ZCC) is the interface between articular cartilage and bone. Pathologic changes in the ZCC associated with osteoarthritis (OA) are identified histologically. These changes involve alterations in tissue integrity and duplication of the tidemark

* Corresponding author at: Orthopaedic Clinic, Medical Faculty, OVGU Magdeburg, Leipziger Strasse 44, 39120, Haus 28 Raum 1.119, Magdeburg, Germany.
E-mail addresses: andrea.schwab@med.ovgu.de (A. Schwab), j.veldman.1@erasmusmc.nl (J. Veldman), n.kops@erasmusmc.nl (N. Kops), wilfred.vanijcken@elembio.com (W.F.J. van IJcken), h.richter@lls-rowiak.de (H. Richter), m.sinram@lls-rowiak.de (M. Sinram), a.dendekker@erasmusmc.nl (X. den Dekker), k.hiscock@erasmusmc.nl (K. Hiscock), jessica.bertrand@med.ovgu.de (J. Bertrand), e.farrell@erasmusmc.nl (E. Farrell), g.vanosch@erasmusmc.nl (G.J. van Osch).

https://doi.org/10.1016/j.joca.2026.05.005

[2,3], the expansion of this zone [4–6], and the invasion of blood vessels [7,8]. However, due to its thin nature and calcified matrix, the ZCC is often overlooked in the characterization and investigation of OA and it is yet not clear if and how the ZCC responds or contributes to the onset of disease and to pathological changes.

One challenge when studying the ZCC is the selective isolation of this layer for analysis. In the osteochondral unit, the tidemark represents the transition of the non-calcified articular cartilage to the ZCC [9–12]. However, the tidemark in the native and fresh tissue is invisible, thus making it practically impossible to visually dissect the ZCC from the adjacent non-calcified articular cartilage without sample processing and staining. The cement line, visible in routine histological staining, marks the transition of the ZCC to the subchondral bone plate, but manually cutting the calcified layers specifically is challenging [13]. Optical Coherence Tomography (OCT) is a promising technology to distinguish between tissues based on the optical density and scattering properties of two tissues, including interfacial tissues. OCT imaging uses near-infrared light to obtain depth-resolved structural information of the tissue. Backscattered light from the sample interferes with a reference light of a known optical path length and generates reflectivity profiles [14].

Characterizing interfacial tissues that are a combination of both soft and a hard tissue, require the use of analytical methodologies compatible with both tissue properties. In contrast to soft tissues, decalcification procedures are usually required to process hard tissues, for example when using laser capture microdissection to collect cells and/or extracellular matrix from a defined region on a tissue section [15,16]. However, fixation, embedding and decalcification reduces RNA quality and yield, thus making these approaches not compatible with transcriptomic studies for the very thin ZCC with a low cell count [17,18].

The aim of this study is to develop methods to enable gene expression and transcriptomic studies of the human ZCC. Our first approach was to set-up an explant culture model to study the *ex vivo* response of the cells in the ZCC to factors associated with inflammation (IL-1β+TNF-α+IFN-γ) and chondrocyte hypertrophy in OA (TGF-β). After demonstrating the sensitivity of the cells in the ZCC to the two stimuli, we set-up a workflow using an OCT-guided 3D-laser microtome to cut the ZCC from non-decalcified osteochondral tissue, enabling us to selectively isolate RNA from the ZCC only. The OCT-guided 3D-laser microtome uses a focused high-frequency laser pulse allowing the precise and contact-free cutting of the selected region from a three-dimensional tissue block of non-decalcified hard tissue [19,20]. Since the ZCC layer contains a low number of cells [21,22], we then use the FLASH-seq technology to successfully sequence the low-input RNA harvested from the laser cut ZCC. The proof-of concept data of the methodological tools established in the two studies show their potential to shed light into the cellular response and the transcriptomic phenotype of the chondrocytes residing in the ZCC in future studies.

Materials and methods

Osteochondral tissue harvest

To develop the *ex vivo* ZCC explant model and to set-up the workflow to isolate and RNA-seq the cells in the ZCC, we harvested osteochondral tissue from eight OA patients (n=4 for explants, n=4 for laser cutting, patient details in Table S1) undergoing total knee replacement surgery (MEC-2021–0595) according to the guidelines of the Medical Ethical Committee of Erasmus MC. The osteochondral tissue was harvested from the macroscopically intact area of the posterior condyles of distal femurs (Table S1), the area being more intact compared to the proximal tibial plateau [23]. The more intact distal femurs were chosen to reduce disease- and load-related variations in the analysis of the ZCC. Moreover, the large area of the distal femurs allowed the harvesting of a higher yield of tissue.

Ex vivo model of the cartilage-bone interface

To study the response of cells in the cartilage-bone interface to stimuli *ex vivo,* we set-up a ZCC explant model. Non-calcified cartilage (NCC) and subchondral bone were cut off from osteochondral tissue (n=4, age between 58 and 77, Fig. 1B, Table S1) and enzymatically digested for complete removal of the NCC (details in supplementary methods). Histological staining and μCT imaging were used to confirm the removal of NCC (details in supplementary). We compared the response of the ZCC explants to donor-matched full thickness NCC explants. The NCC explants were kept overnight in DMEM LG (Gibco) supplemented with 10% FCS (Sigma-Aldrich) and antibiotics (gentamycin: 50 μg/ml, amphotericin B: 1.5 μg/ml, Gibco), washed with saline and transferred into well plates. Explants were cultured in basic media (DMEM low glucose (LG), 1% ITS$^+$ (Corning), antibiotics) for six days and stimulated for three days with a pro-inflammatory cytokine cocktail (IL-1β, TNF-α and IFN-γ, 1 ng/ml each) or with TGF-β1 (10 ng/ml, recombinant human, R&D Systems) in basic media. After 72 h of explant stimulation samples were harvested and nitric oxide (NO) and ALP released into the culture media was measured.

Gene expression analysis

Tissues of the explant cultures were snap frozen, pulverized (Mikro-Dismembrator, B. Braun Biotech International GmbH), homogenized with RNA STAT-60 (Gentaur) and mixed with chloroform for phase separation. Total RNA was isolated using EconoSpin mini columns (Epoch Life Science) in combination with buffers from RNeasy Micro Kit (Qiagen). RNA was quantified, transcribed into cDNA and quantitative polymerase chain reaction was done using a standard protocol (primer sequence and PCR details in supplementary tables). The best keeper index (BKI) was calculated from the C_t values of the reference genes (*GAPDH, UBC* and *HPRT*) to correct the C_t values of the selected genes of each respective sample. Samples with no Ct value and samples with a $C_t \geq 36$ were considered undetectable and set to 40 for further calculation. Relative gene expression was calculated using $2^{-\Delta Ct}$ method and average values of biological replicates were plotted.

Statistical analysis of the explant culture

Replicate values were averaged and all data was plotted and statistical analyses performed using GraphPad Prism (Version, 10.4.1). Differences between groups were determined using either paired t-test or repeated measures ANOVA with matched samples and Dunnett´s multiple comparison test. Matched sample Friedman test with Dunn´s multiple comparison test was used for non-parametric data. A p-value of $p < 0.05$ was considered significant.

Histological processing and staining

Samples were fixed (4% formalin, Carl Roth), decalcified (10% EDTA), paraffin embedded and sectioned. Safranin-O staining (details in supplementary methods) was used to visulaize the ZCC. Immuno-histochemical staining for sclerostin and collagen type II (details in supplementary methods) were used to verify FLASH-seq results.

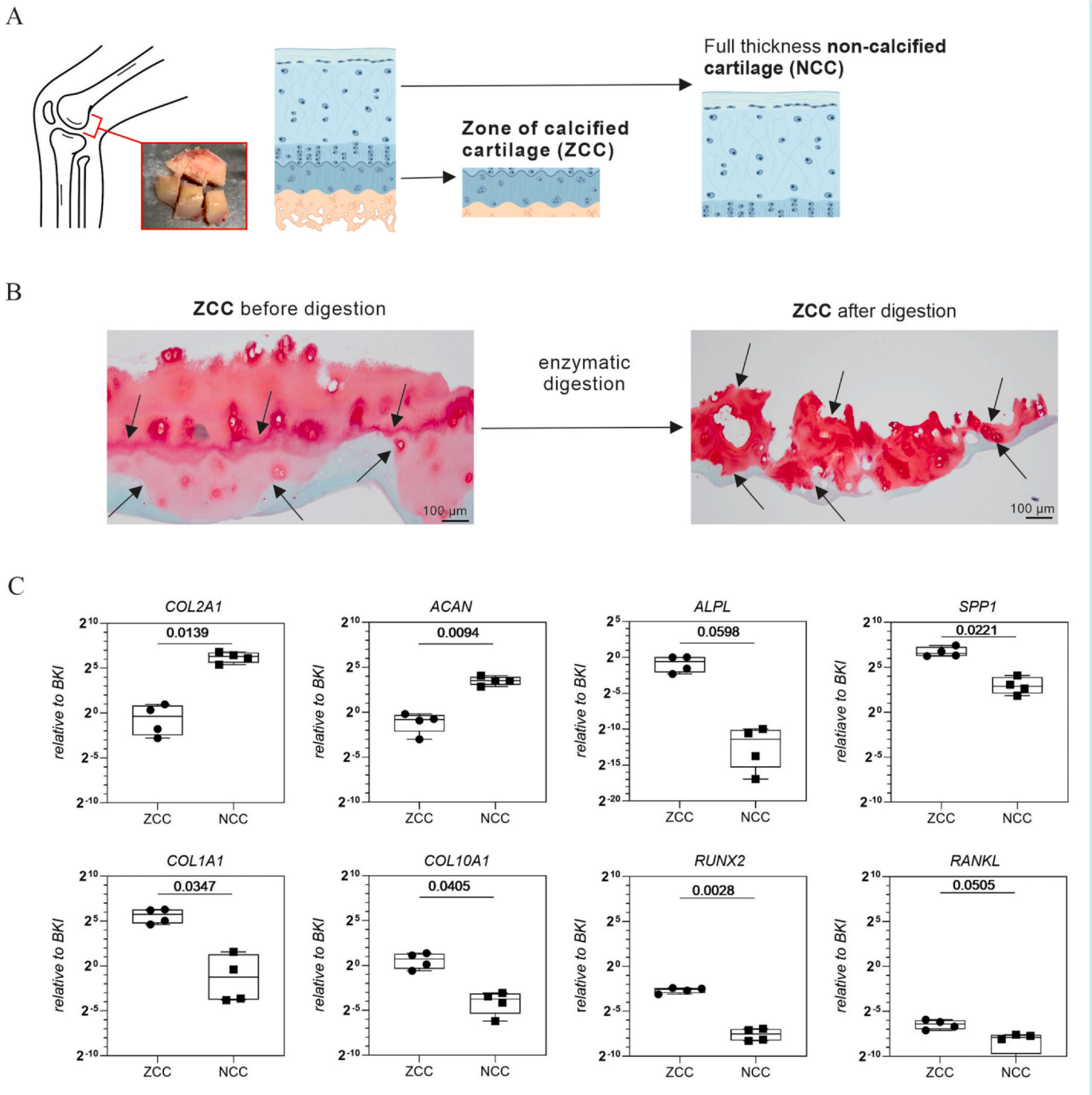

Fig. 1

Osteoarthritis and Cartilage

Development of the *ex vivo* model of the zone of calcified cartilage (ZCC). (A) Schematic illustration of the tissue harvest and the isolation of the ZCC explants and the full-thickness non-calcified cartilage (NCC) explants from human osteochondral tissue. (B) Safranin-O staining of ZCC explants before (native) and after mild enzymatic treatment to remove remaining non calcified cartilage left on the ZCC explants after manual dissection. The tidemark appears as red line-like structure in the safranin-O positive area before digestion and is no longer visible after digestion. The area of the ZCC is marked with black arrows. Scale bar 100 µm. (C) qRT-PCR gene expression data of ZCC and NCC explants cultured in control media (day 10). The best keeper index (BKI) was calculated from the reference genes GAPDH, HPRT and UBC. Paired t-test of n=4 donors, each dot represents the average of n=1–3 samples per donor and explant group. A p-value of $p < 0.05$ was considered significant. Box plot (min. to max.) with line at mean. 95% CI *COL2A1* [29.84–124.60]; *COL10A1* [-2.99–0.13]; *ACAN* [5.20–17.10]; *ALPL* [-1.34–0.05]; *SPP1* [-174.20–27.52]; *RUNX2* [-0.21–0.10]; *COL1A1* [-96.03–6.98]; *RANKL* [-0.02–3.62e-5].

OCT-guided 3D-laser microtomy

To enable the characterization of the transcriptome of the cells residing in the ZCC, we used a combination of two innovative technologies, the OCT-guided 3D-laser microtomy and the RNA FLASH-seq analysis. Fresh osteochondral tissue was harvested as described before. In the laboratory, osteochondral tissue was cut (cube size 1 cm^3, n= 4, age between 60 and 86, Table S1) and stored in RNAlater® at 4°C (Ambion, Biocompare) to preserve the RNA of the fresh tissue blocks. Tissue cubes were trimmed with a diamond saw (Secotom-15, Struers) to prepare a plane surface and placed in a custom-made acrylic ring. OCT imaging of the laser microtome (TissueSurgeon, LLS ROWIAK LaserLabSolutions GmbH) was used to identify the area of interest, the ZCC. After 3D-laser cutting the area of interest (cutting depth: 80 µm, cutting energy: 180 nJ), the cut tissue was collected in Trizol (QIAzol, QIAGEN) on ice, snap frozen and stored at −80°C till RNA was isolated. The respective deep zone of the non-calcified cartilage (dNCC) tissue were laser cut accordingly as comparative controls.

RNA-sequencing

RNA isolation of laser cut ZCC and dNCC was done by phase separation using chloroform. RNA was precipitated in isopropanol, washed with Ethanol (75%), dissolved in RNAse free water and stored at −80°C. The FLASH-seq bulk workflow [24,25], a modified version of the FLASH-seq single cell method (details in supplementary methods), was used to prepare transcriptome libraries from total RNA (laser cut samples: ZCC, dNCC, Explant cultures: interface and cartilage +/-TGF-β1), followed by tagmentation of 400 pg of cDNA. Sequencing was performed on the NextSeq 2000 (Illumina) with 50 bp paired-end reads. Data was analyzed using a Snakemake pipeline (v 6.11.0) and adapters were trimmed with Cutadapt (v 3.6) [26,27]. Reads were aligned to GRCh38 using STAR (v 2.7.9a) and gene expression matrix was generated with STARsolo [28,29].

Bioinformatic analysis and statistics

Raw counts and metadata were loaded into R (v4.3.1) using Matrix(v1.6–5) and readr (v2.1–5) packages. Standard DESeq2 (v1.40.2) analysis was performed using a model including donor, tissue type or treatment as covariates depending on the experimental set up. Normalization using variance-stabilizing transformation was applied and principal component analysis (PCA) plots generated to assess sample variance. Differential expression (DE) analysis was performed and genes with unadjusted p-value < 0.05 and log2 fold changes > 0.5 were considered differentially expressed. The unfiltered list of genes was ranked by their Wald statistic and the entire list was used for input for Gene Ontology (GO) gene set enrichment analysis using clusterProfiler package (v4.8.3). Significantly enriched pathways were identified based on Normalized Enrichment Scores (NES). All data was visualized using ggplot2 (v3.5.1).

Results

We developed a ZCC explant model using macroscopically intact tissue of the posterior part of the distal femurs of four OA patients (Fig. 1A, Table S1). The ZCC explants were composed of the ZCC with a thin layer of the adjacent subchondral bone and the NCC was removed as confirmed by µCT imaging (Figure S1). The area of the attached subchondral bone varied with the waviness of the cement line and showed an overall similar thickness to the ZCC. Histological staining confirmed the removal of residues of bone marrow in the trabecular space and the removal of the bone lining cells. The adjacent deep layer of the NCCwas removed after the enzymatic treatment with the tidemark defining the upper boundary of the ZCC interface explants (Fig. 1B).

We then assessed the expression of selected genes associated with chondrocytes and hypertrophy by qPCR. We compared the gene expression of the cells residing in the ZCC explants to the donor-matched NCC explants without the ZCC (Fig. 1C). ZCC explants showed a higher relative expression of *COL10A1*, *COL1A1*, *RANKL* and *SPP1* compared to NCC cultured in control media and a strong trend for *RANKL*. *COL2A1* and *ACAN* were less expressed in the ZCC explants compared to the NCC explants when cultured in control media. *ALPL* was expressed in ZCC explants, but not detected in the NCC explants.

The cells residing in the ZCC explants responded with clear differences between the stimuli to which they were exposed (Fig. 2A). The ZCC and NCC explants both responded with an increase in *IL6* after stimulation with the cytokine mix compared to the respective control sample. *MMP13* was expressed by the explants stimulated with cytokines whereas no or very low expression was detected in the control groups. The cytokine treatment lowered the expression of *SPP1* in ZCC explants, while the NCC explants responded with a decrease in *RUNX2* (Figure S2) and no change in the expression of *SPP1*. NCC explants responded with a decrease in *ACAN* and *COL2A1* upon cytokine stimulation. ZCC explants did not show a response in *ACAN* and *COL2A1.* The cytokine cocktail did not change *COL1A1, COL10A1, or ALPL* in NCC nor ZCC explants.

ZCC explants responded to the addition of TGF-β1 with an increase in *COL10A1* compared to the respective control explants, whereas the TGF-β1 stimulation did not change *COL10A1* expression in NCC explants (Fig. 2A). ZCC and NCC explants showed a similar trend for all other genes with no change in the expression of *COL2A1*, *ACAN*, *COL1A1*, *SPP1*, *ALP, MMP13,* and *SPP1* in response to TGF-β1 compared to the respective control groups. To evaluate the use of FLASH-seq for bulk analysis of these samples (Figure S3), we analyzed the TGF-β1 samples with this methodology. The FLASH-seq bulk results showed a similar trend (Figure S4-S6) in comparison to the qPCR data. Additionally, we quantified the release of NO and ALP released to the culture media. The TGF-β1 stimulated NCC explants showed an increase in NO compared to the control group. ALP was not released from any of the explants (Fig. 2B). The qPCR and FLASH-seq data demonstrated that the cells residing in the ZCC explants respond to stimuli associated with OA.

Next, we set-up a workflow to isolate the ZCC from fresh human osteochondral tissue (Fig. 3A) and to run FLASH-seq bulk analysis. ZCC enriched and donor-matched deep zone of the non-calcified articular cartilage (dNCC) were isolated using an OCT-guided 3D-laser microtomy from human tissue samples that were not decalcified (Fig. 3A). The dNCC controls were used to reduce confounders in the data analysis resulting from the heterogeneity of chondrocyte sub-populations in the different zones. OCT imaging integrated into the 3D-laser microtome was used to identify the ZCC in osteochondral tissue (Fig. 3B). 2D OCT images before and after the laser cutting (laser cut area highlighted in red) allowed the verification of location of the planar cut (Fig. 3C). The safranin-O-stained sections showed the successful laser cutting and isolation of the ZCC leaving an empty space in the area of the ZCC (Fig. 3D). Further histological staining and OARSI scores of the laser cut tissue indicate first signs of proteoglycan loss and tidemark duplication (Figure S7).

We successfully sequenced RNA from the two laser-cut tissue types (ZCC and dNCC). The high number of detected features (genes) and the sequencing depths across all samples (Fig. 4A) suggested a good coverage of the transcriptome. The PCA plots showed a high similarity between dNCC and ZCC. Within PC2 a separation of the two tissue types with some overlap of the two tissue types can be seen (Fig. 4B). We identified 484 genes that were higher expressed and 434 genes that were lower expressed in the 3D-laser cut ZCC

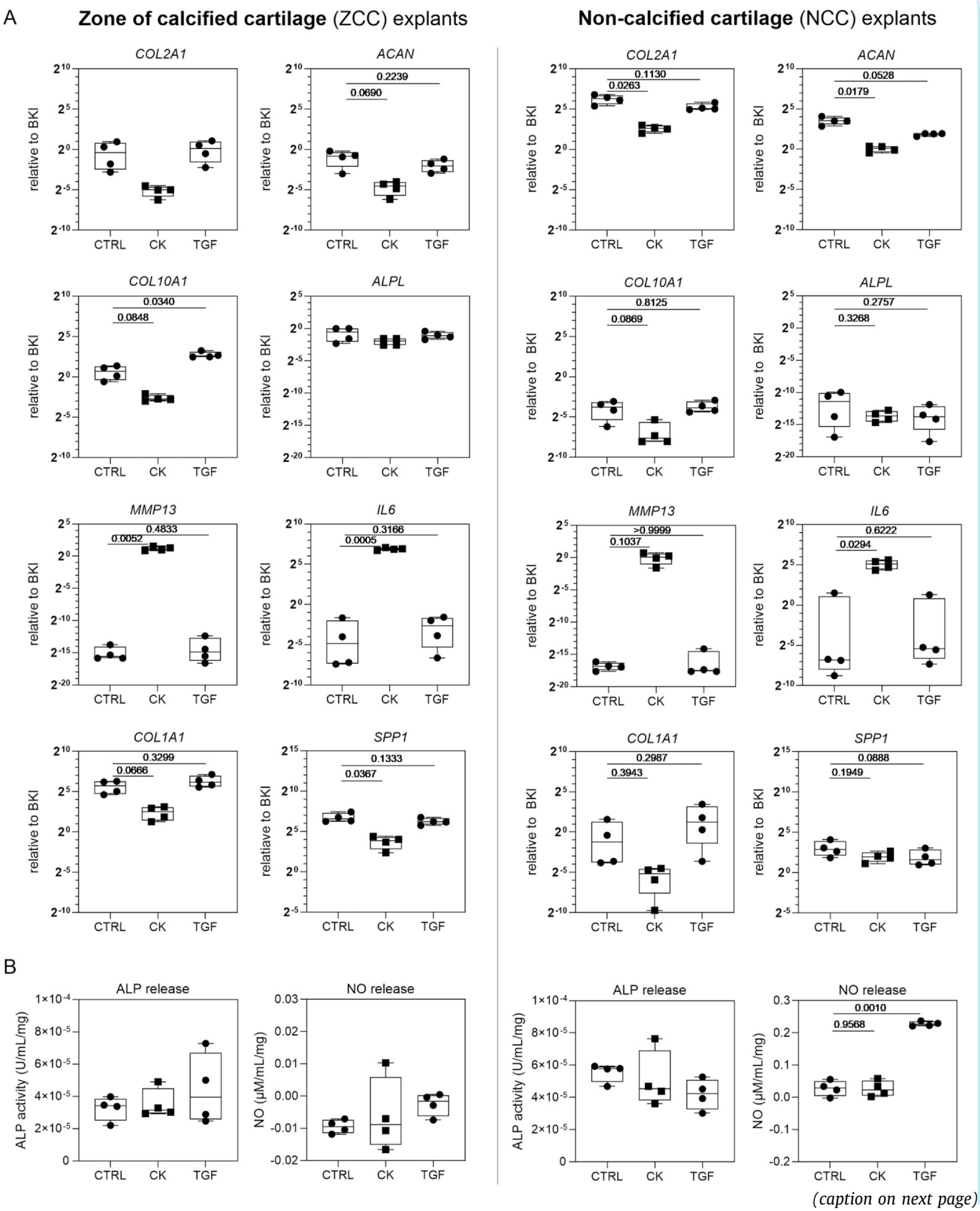

(caption on next page)

Fig. 2 Osteoarthritis and Cartilage

Response of explants of the zone of calcified cartilage (ZCC) and full thickness non-calcified cartilage explants (NCC) to the osteoarthritic associated factors, a pro-inflammatory cytokine cocktail (CK: TNF-α, INF-γ, IL-1β, 1 ng/ml each) or TGF-β1 (TGF, 10 ng/ml). ZCC and NCC explants were stimulated for 72 h. (A) qRT-PCR gene expression of ZCC and NCC explants in response to the CK treatment and TGF treatment is expressed relative to the best keeper index (BKI), a set of three reference genes *GAPDH, HPRT* and *UBC*. The main responding genes in the CK treatment were *MMP13* and *IL6* while *COL10A1* was the most responsive genes in the TGF stimulated explants. (B) Release of alkaline phosphatase (ALP) and nitric oxide (NO) of NCC and ZCC explants into the media supernatant. Repeated measures ANOVA of donor-matched samples with Dunnett´s multiple comparison test (gene expression except *MMP13* cartilage explants), repeated measures ANOVA of donor-matched with Šídák's multiple comparison test samples (NO release cartilage and interface explants, ALP release interface explants) and Friedman test with Dunn´s multiple comparison test (*MMP13* cartilage explants, *ALPL* interface explants, ALP release cartilage explants). n=4 donors, each dot presents the average data of n=1–3 samples per donor and treatment). A p-value of $p < 0.05$ was considered significant. Box plot (min. to max.) with line at mean. 95% CI [95% CI CK vs CTRL / 95% CI TGF vs CTRL]. ZCC: *COL10A1* [-3.28–0.35 / 0.71–9.60]; *ACAN* [-1.06–0.07 / −0.80–0.26]; *SPP1* [-181.00 to −10.71 / −81.47–16.53]; *MMP13* [1.29–3.34 / −0.76e-6–0,14e-3]; *RUNX2* [-0.18 to −0.02 / −0.14–0.18e-2]; *COL1A1* [-99.47–5.675 / −43.90–104.00]; *RANKL* [-0.05–0.02 / −0.07–0,73e-3]; *IL6* [94.72–142.80 / −0.10–0.23]. NCC: *COL2A1* [-128.05 to −15,56 / -93.83–15.66]; *COL10A1* [-0.14–0.15 / −0,05 to 0,07]; *ACAN* [-17.89 to −3.38 / −16.33–0.17]; *ALPL* [-0.12e-3–0, 51e-3 / −0.11e-2–0, 40e-3]; *SPP1* [-13.44–3.89 / −10.71–1.24]; *RUNX2* [-0.01 to −0.91e-6 / −0.01–0.01]; *COL1A1* [-3.61–1.704 / −3892 to 9839]; *RANKL* [-0.01–0.21e-2 / −0.01–0.03]; *IL6* [6.11–60.90 / −0.53–0.33]; *MMP13*: rank sum difference [5.50 / −1.00]; NO release [-0.01–0.01 / 0.15–0.25].

compared to the dNCC (Fig. 5A). A heatmap of the top 50 DE genes is provided in the supplementary (Figure S8). Similar to the finding in the explant culture model, *COL2A1, ACAN* and *SOX9* were differentially expressed between the two tissues, in the differential expression analysis between ZCC and dNCC. Interestingly, the hypertrophy-associated genes (*COL10A1, ALPL, SPP1*) were not differentially expressed comparing ZCC and dNCC (Fig. 5B).

The GO term pathway analysis comparing the NES resulted in six pathways that were positively regulated and 14 pathways that were negatively regulated in the ZCC compared to the dNCC (Fig. 5C, Figure S9). MHC class II associated GO Terms were among the top positively regulated pathways in the ZCC compared to dNCC. Pathways related to mRNA splicing, ribosome, and metabolic process were among the negative regulated pathways in the ZCC compared

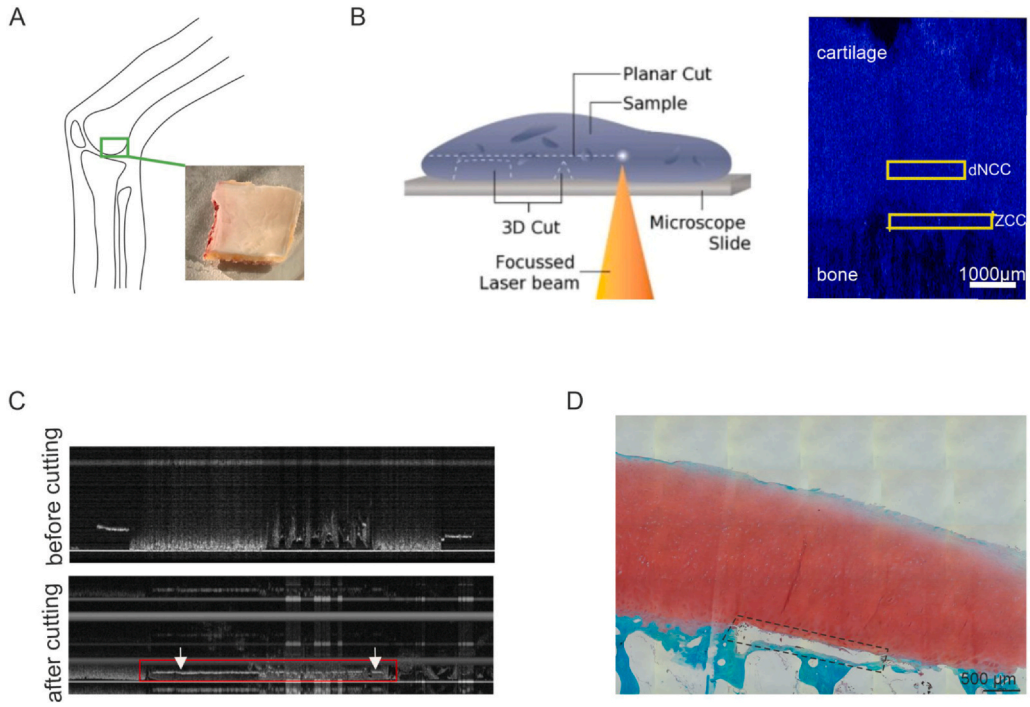

Fig. 3 Osteoarthritis and Cartilage

Establishment of the workflow to isolate the zone of calcified cartilage (ZCC) from human osteochondral tissue and RNA bulk sequencing analysis. (A) Human osteochondral tissue blocks were harvested from distal femurs. (B) Schematic drawing of the 3D-laser cutting principle and a representative 3D-optical coherence tomography (OCT) image of the osteochondral cross section. 3D-OCT images were used to select the region of interest in non-calcified cartilage deep layer (dNCC) and the ZCC indicated with yellow rectangles. (C) 2D-OCT images of the osteochondral tissue before and after laser cutting. White arrows in the 2D-OCT image after cutting point at the planar cut. (D) Safranin-O stained tissue section to confirm the successful laser cutting of the ZCC (black dashed line). Scale bar 500 µm.

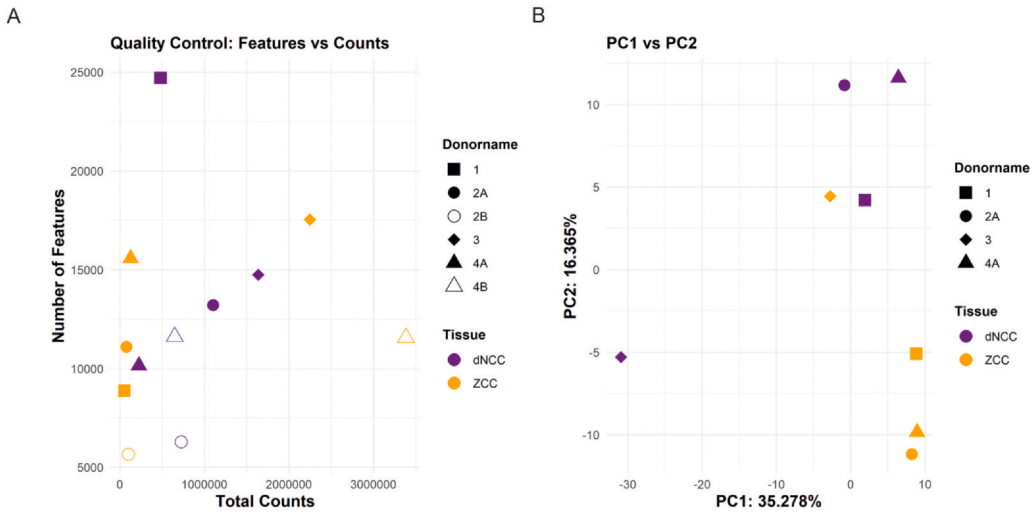

Fig. 4

Osteoarthritis and Cartilage

Bulk RNA FLASH-seq results of the zone of calcified cartilage (ZCC) and the adjacent deep zone non-calcified articular cartilage (dNCC). (A) The RNA isolated from the two laser-cut tissue types (ZCC and dNCC) from at least one replicate of each of the four donors was successfully sequenced with a good coverage of the transcriptome. RNA quality of the laser cut tissue is displayed by total counts versus number of genes (features). (B) PCA plot of top two principal components (PC) showed a high similarity between the dNCC and ZCC. n=4 donors.

to dNCC. The GO term "regulation of cell migration involved in sprouting angiogenesis" was negatively regulated in the ZCC compared to dNCC. Among others, *VEGFA* and *ANXA1* are two genes of this pathway with a higher gene count in the dNCC compared to the ZCC. These data indicate that chondrocytes in the ZCC have a phenotype similar to the chondrocytes in the dNCC, albeit with a clear difference in the expression of angiogenic factors.

To validate that we have isolated specifically the ZCC, the RNA-seq data did not show the expression of osteocyte-associated genes (Figure S10). Moreover, one of the highest differentially expressed genes between ZCC and dNCC was *SOST*, the gene coding for sclerostin (Fig. 5A). Immunohistochemical staining for sclerostin and collagen type II confirmed the RNA-seq data. Chondrocytes in the ZCC and subchondral bone were positively stained for sclerostin. The articular cartilage including the ZCC were positively stained for collagen type II (Fig. 6). The workflow of the two technologies has shown its potential in isolating cells from a specific zone within the osteochondral unit, in this case the till now largely neglected ZCC. This spatially resolved analytical approach offers the possibility to study the role of the cells in the ZCC in health and in disease.

Discussion

The dense mineralized ZCC comprises only 3–8% of the total articular cartilage volume [30] with an average thickness ranging between 75 and 250 μm in humans [3,22]. The number of cells in the ZCC is low (30–70 cells per mm²) compared to the chondrocyte density in NCC (120–530 cells per mm²) [21,22]. Cells residing in the ZCC are often described as having a hypertrophic phenotype [11,31] and might possibly play a role in OA disease progression. However, the role of the cartilage-bone interface in OA onset and OA progression, specifically the ZCC, at a cellular level remains understudied. The main reasons are the challenges related to analysis of this calcified, low cell density tissue. In this study, we have established an *ex vivo* explant model of the ZCC. Additionally, we have set-up a workflow allowing the selective isolation of the ZCC and we used the FLASH-seq technology to analyse the low amount of RNA isolated from this tissue. These technologies provided a proof-of-principle approach that will generate new hypotheses on the role of the ZCC in OA.

The *ex vivo* human ZCC explant model allows the study of the response of cells residing in this zone to stimuli associated with OA such as TGF-β or pro-inflammatory cytokines. Investigations on the role of the cartilage-bone interface in the pathogenesis of OA are scarce. To our knowledge, the data of the ZCC explant model are the first results in literature showing that the chondrocytes residing in the ZCC are sensitive to external stimuli *ex vivo*. Chondrocytes in the ZCC explants responded to external stimuli associated with OA disease, thus indicating that the cells in this layer are metabolically active and potentially play a role in OA disease. The ZCC explants and the NCC explants showed a tissue specific response to the two OA-associated stimuli. Chondrocytes from OA patients respond to TGF-β stimuli with an increase in *COL10A1* and can undergo calcification *in vitro*, whereas TGF-β does not activate healthy articular chondrocytes to become collagen type X expressing cells [32–36]. Our data suggest that the cell population in the ZCC explants are more susceptible to TGF-β than chondrocytes in NCC explants. Moreover, our data suggests that cells in ZCC and NCC explants respond with an increase in collagen type X, similarly to hypertrophic OA chondrocytes.

A limitation of this model is that it does not purely consist of ZCC, since the explants contain a small layer of the adjacent subchondral bone plate. Although the number of bone cells is relatively small, we cannot exclude their influence on the results. In future studies, the OCT-guided 3D-laser dissection of the ZCC might be used for more specific information on cells from ZCC explants exclusively. Another limitation of our set-up is that we used intact tissue from the less loadbearing posterior part of the femur condyles. The explant isolation and *ex vivo* culture might have affected the gene expression of the cells in the ZCC. In future studies, the response of ZCC explants from the load-bearing areas of the femur or the tibia, also including explants from patients with different severity of OA could be used.

Our model opens new possibilities to increase our knowledge of the soft-hard tissue interface, and particularly the ZCC, in OA. This *ex vivo* model is affordable and has the potential to be used as a

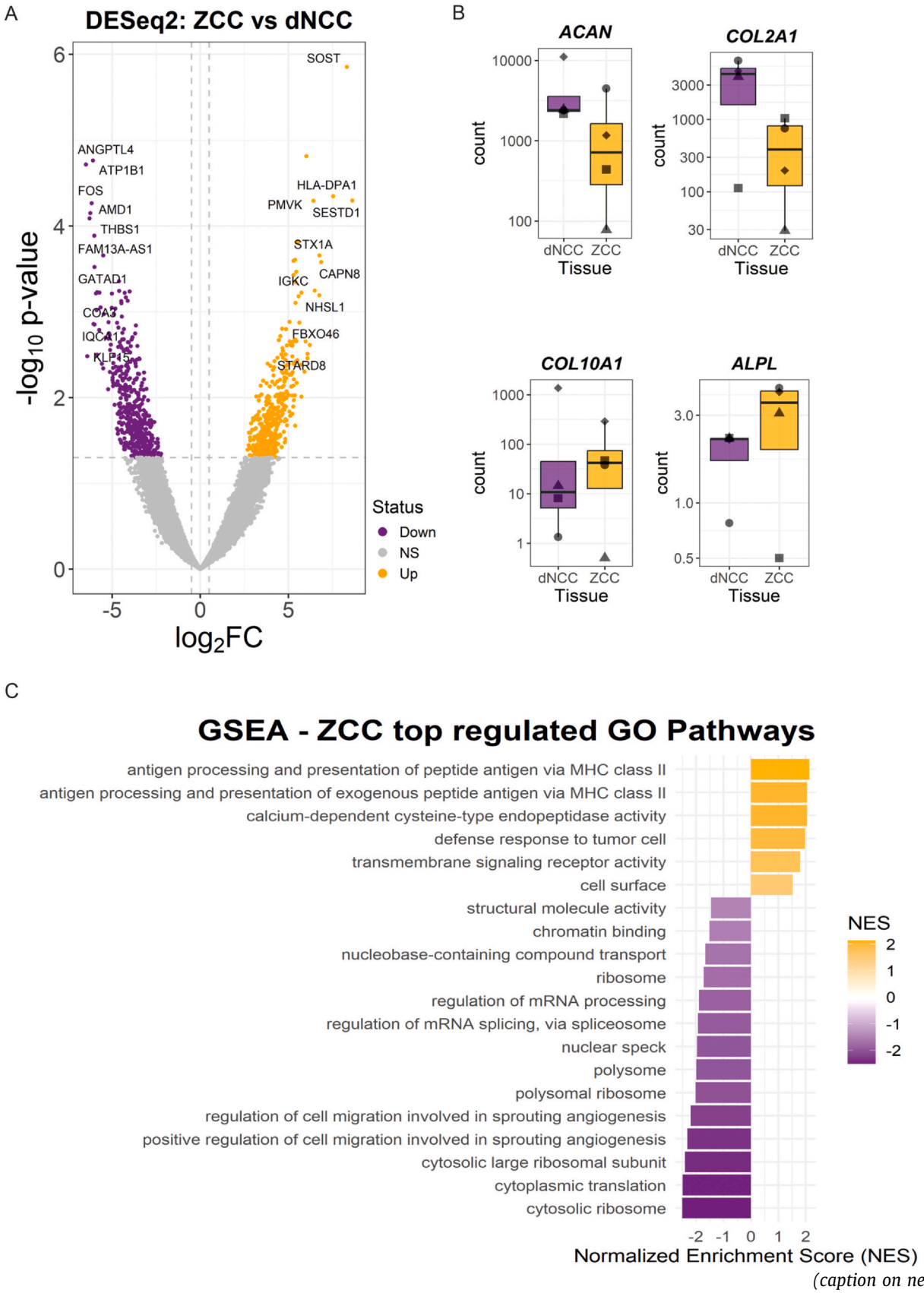

(caption on next page)

Fig. 5 Osteoarthritis and Cartilage

Donor-matched (paired) expression profile comparison of the chondrocytes in the zone of calcified cartilage (ZCC) and the deep zone of non-calcified articular cartilage (dNCC) using the FLASH-seq bulk analysis. (A) Differential expression (DE) analysis comparing the ZCC to dNCC (Purple: lower expressed in ZCC vs dNCC, orange: higher expressed in ZCC vs dNCC, grey: no significant differences). *SOST* (log2FC ± lfcSE of 8.31 ± 1.72, $p < 0.0001$) was the highest differentially expressed gene in ZCC vs dNCC while *ANGPTL4* (log2FC ± lfcSE of -6.08 ± 1.42, $p < 0.0001$) was the highest differentially expressed gene in dNCC vs ZCC. (B) DE of selected cartilage-associated genes (*ACAN* p=0.041, COL2A1 p=0.011, *SOX9* p=0.040) and hypertrophy-associated genes (*COL10A1* p=0.841, *ALPL* p=0.661, *SPP1* p=0.406) comparing dNCC and ZCC. (C) Gene ontology (GO) pathway analysis of the ZCC compared to dNCC. n=4 donors, donor-matched paired analysis. A p-value of $p < 0.05$ was considered significant. The gene count data of the RNA-seq analysis is available open access on Dataverse.

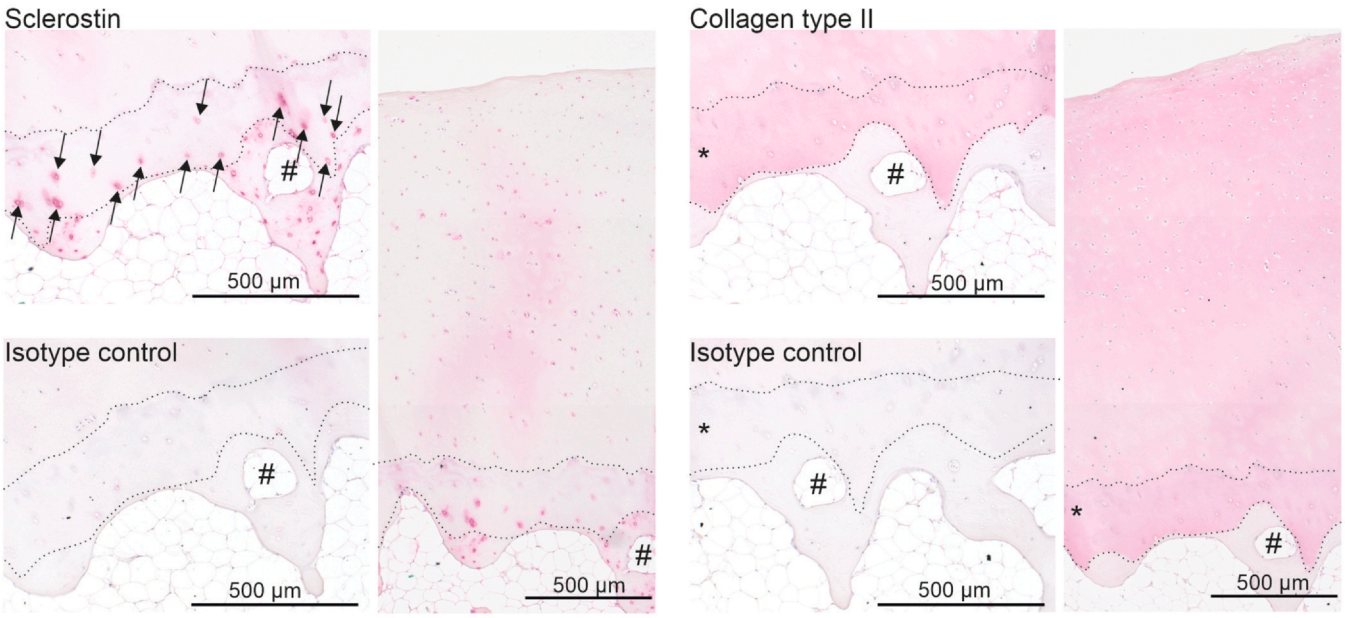

Fig. 6 Osteoarthritis and Cartilage

Representative immunohistochemical stainings (sclerostin and collagen type II) of osteochondral tissue (donor 3) used for the 3D-laser microtomy and RNA FLASH-seq analysis. Overview image of the osteochondral unit and zoom in into the deep zone of the non-calcified cartilage, zone of calcified cartilage (ZCC) and subchondral bone. Respective isotype controls for each antibody are shown for the zoom in images. The purple staining indicates a positive antibody staining. Dashed lines indicate the tidemark and the cement line. # indicates a reference point in all images. Arrows point on sclerostin positive stained cells in the ZCC. * indicates the ZCC in the collagen type II staining.

medium to high throughput platform, allowing for the study of cellular response to various stimuli and pharmacological treatments in an *ex vivo* setting. The model can be used to study the response of the cartilage-bone interface from patients with varying OA severity and might help to develop interventions to inhibit disease progression and including healthy interfaces would be possible when transferring the model to other species.

OCT-imaging-guided 3D-laser microtomy and FLASH-seq bulk sequencing are two innovative technologies overcoming the limitation of standard approaches to laser cut the thin interfacial ZCC layer followed by sequencing low input RNA. The OCT-imaging of the laser microtome allows the discrimination between cartilage, ZCC and bone tissue. Moreover, the OCT-guided 3D-laser microtome does not require tissue processing (e.g. paraffin embedding or decalcification) known to lower gene expression and RNA quality [17,18]. The use of the FLASH-seq technology, a single cell RNA-sequencing method with high sensitivity and specificity [25,37], overcame the challenge in the analysis of the low amount of RNA that can be harvested from the thin ZCC [3,22,30]. The limited access to these devices and technologies, mainly restricted to specialized core-facilities, and the high costs to process and analyse the samples are the main limitation.

Since this is the first-time gene expression data, specifically on cells enriched from the ZCC, extensive comparison of our data with literature is not possible. Our data suggest a similarity of the cell phenotype between chondrocytes in the dNCC and ZCC. During cartilage maturation, the deep zone cartilage mineralizes and forms the ZCC upon skeletal maturity, explaining the similarity of the two chondrocyte subpopulations [38,39]. The RNA-seq data on the ZCC revealed no differential expression of *ACAN* in the ZCC compared to the dNCC control tissue, while *ACAN* was lower in the ZCC explants compared to NCC explants used in the culture model. The choice of control tissues, full-thickness NCC in the explant cultures and dNCC in the 3D-laser microtome approach, might explain this difference. Moreover, *in vitro* cultured deep zone chondrocytes express lower levels of *ACAN* compared to chondrocytes isolated from the superficial zone (passage 0) of human articular cartilage [40,41]. Interestingly, cells in the ZCC expressed a low level of *COL10A1* and

COL10A1 was not differentially expressed between ZCC and dNCC. Hypertrophic chondrocytes in the ZCC showed a high *COL2A1* and *ACAN* gene count, that have not been reported to be specific for hypertrophic and collagen type X expressing chondrocytes in growth plate cartilage [42,43].

Despite the similarities between ZCC and dNCC, these chondrocytes showed a clear differences in *SOST* expression and angiogenesis sprouting-associated gene expression (e.g. *VEGFA*, *ANXA1*), thus being candidate genes to differentiate between the two chondrocyte sub-populations. Sclerostin is a negative regulator of bone growth and it inhibits canonical WNT signalling, suggesting a protective effect to prevent the matrix from transitioning towards bone at this interface [44–46]. Chondrocytes in mineralized cartilage and hypertrophic chondrocytes in OA can express *SOST*, thus its expression is not limited to osteocytes [47–49]. The GO terms related to angiogenesis indicate an increased likeliness of invasion of blood vessels in the avascular cartilage dNCC compared to the ZCC during OA, one of the pathological changes in the osteochondral unit [7,8]. Moreover, it has been shown that healthy articular cartilage also releases pro-angiogenic factors [50].

The ZCC explant model, the workflow to selectively isolate the ZCC and the first RNA-seq data of the ZCC are tools to get a more complete picture of the ZCC in follow-up studies. The methodological approach can also be translated to other calcified tissues. The initial biological data obtained from the methodological approach to study the ZCC showed similarities and differences between the ZCC and dNCC. Additional validation of the proof-of-concept data and a more in-depth analysis of the ZCC in future studies with a larger sample size is recommended to reveal the novel insights on this layer that is barely studied until now. Tissues harvested from the load-bearing area of the proximal tibia as well as a comparison of different OA severity and sex-differences can be studied in follow-up experiments.

Most importantly, both methodological approaches, the explant culture model and the OCT-guided 3D-laser microtome on non-decalcified tissues, can be combined to investigate hypothesis and research questions generated from our proof-of-concept data. Using these techniques in future studies will generate new biological insights into the phenotype of the hypertrophic chondrocytes residing in the ZCC and its contribution to the development of OA.

Author contributions

Conception and design: AS, WIJ, HR, MS, EF, GVO, Analysis and interpretation of the data: AS, JV, NK, HR, MS, XDD, KH, JB, EF, GVO, Drafting of the article: AS, JV, GVO, EF, Critical revision of the article for important intellectual content: NK, WIJ, HR, MS, XDD, KH, JB, Final approval of the article: all, Statistical expertise: JV, XDD, KH, Obtaining of funding: AS, GVO, EF, Administrative, technical, or logistic support: JV, NK, MS, HR, Collection and assembly of data: AS, JV, NK, XDD, KH, MS, HR.

Role of funding

The work was funded by the Health Holland TKI of the Erasmus MC, University Medical Center Rotterdam (EMCLSH20022), the Deutsche Forschungsgemeinschaft (DFG, German Research Foundation no. DFG SCHW 2116/1-1). The authors like to thank the Dutch Arthritis Society (LLP34) and the COST action CA211100 NetwOArk. Dutch Arthritis Society (LLP34) and COST action CA211100 NetwOArk.

Data availability

The raw and processed data of culture experiment (qPCR, NO and GAG) are available as supplementary information. The RNA-seq data are available at DataverseNL, V1, http://doi.org/10.34894/HW5K0O.

Declaration of Competing Interest

The authors have no conflicts of interest to declare.

Declaration of Generative AI and AI-assisted technologies in the writing process

During the preparation of this work the authors used Microsoft Copilot and BLACKBOX AI in order to optimize and refine script coding in R. After using this tool, the author reviewed and edited the content as needed and take full responsibility for the content of the manuscript.

Acknowledgements

We thank the Department of Orthopaedics of the Elisabeth-TweeSteden Ziekenhuis (ETZ) in Tilburg for providing osteochondral tissues from patients undergoing knee replacement surgery. The authors thank Anja Schröder (OVGU Magdeburg) for the histological processing of the samples. This work is part of the Convergence Flagship Healthy Joints and the International Network on Ectopic Calcification (INTEC).

Appendix A. Supporting information

Supplementary data associated with this article can be found in the online version at doi:10.1016/j.joca.2026.05.005.

References

[1] W. Badar, S.R. Inamdar, P. Fratzl, T. Snow, N.J. Terrill, M.M. Knight, et al., Nonlinear stress-induced transformations in collagen fibrillar organization, disorder and strain mechanisms in the bone-cartilage unit, Adv. Sci. (Weinh.) 12 (2025) e2407649, https://doi.org/10.1002/advs.202407649
[2] D. Palmer, W.D. Strain, B. Webb, 242. Turning of the tide: does tidemark advancement perpetuate osteoarthritis, Rheumatology 53 (2014), https://doi.org/10.1093/rheumatology/keu118.002 i150-i150.
[3] L.B. Lane, P.G. Bullough, Age-related changes in the thickness of the calcified zone and the number of tidemarks in adult human articular cartilage, J. Bone Jt. Surg. Br. 62 (1980) 372–375, https://doi.org/10.1302/0301-620X.62B3.7410471
[4] L.B. Hartlev, R. Klose-Jensen, J.S. Thomsen, J.R. Nyengaard, L.W.T. Boel, M.B. Laursen, et al., Thickness of the bone-cartilage unit in relation to osteoarthritis severity in the human hip joint, RMD Open 4 (2018) e000747, https://doi.org/10.1136/rmdopen-2018-000747
[5] X. Fan, X. Wu, L. Trevisan Franca De Lima, S. Stehbens, C. Punyadeera, R. Webb, et al., The deterioration of calcified cartilage integrity reflects the severity of osteoarthritis-a structural, molecular, and biochemical analysis, FASEB J. 36 (2022) e22142, https://doi.org/10.1096/fj.202101449R
[6] R. Klose-Jensen, L.B. Hartlev, J.S. Thomsen, J.R. Nyengaard, L.W.T. Boel, M. Laursen, et al., Calcified cartilage in patients with osteoarthritis of the hip compared to that of healthy subjects. A design-based histological study, Bone 143 (2021) 115660, https://doi.org/10.1016/j.bone.2020.115660
[7] S. Suri, S.E. Gill, S. Massena de Camin, D. Wilson, D.F. McWilliams, D.A. Walsh, Neurovascular invasion at the osteochondral junction and in osteophytes in osteoarthritis, Ann. Rheum. Dis. 66 (2007) 1423–1428, https://doi.org/10.1136/ard.2006.063354
[8] D.A. Walsh, D.F. McWilliams, M.J. Turley, M.R. Dixon, R.E. Fransès, P.I. Mapp, et al., Angiogenesis and nerve growth factor at the osteochondral junction in rheumatoid arthritis and osteoarthritis, Rheumatology (Oxford) 49 (2010) 1852–1861, https://doi.org/10.1093/rheumatology/keq188
[9] P.A. Simkin, A biography of the chondrocyte, Ann. Rheum. Dis. 67 (2008) 1064–1068, https://doi.org/10.1136/ard.2007.084574
[10] E. Dmitrovsky, L.B. Lane, P.G. Bullough, The characterization of the tidemark in human articular cartilage, Metab. Bone Dis. Relat. Res. 1 (1978) 115–118, https://doi.org/10.1016/0221-8747(78)90047-4

[11] L.A.E. Evans, A.A. Pitsillides, Structural clues to articular calcified cartilage function: a descriptive review of this crucial interface tissue, J. Anat. (2022), https://doi.org/10.1111/joa.13728
[12] K.P. Pritzker, S. Gay, S.A. Jimenez, K. Ostergaard, J.P. Pelletier, P.A. Revell, et al., Osteoarthritis cartilage histopathology: grading and staging, Osteoarthr. Cartil. 14 (2006) 13–29, https://doi.org/10.1016/j.joca.2005.07.014
[13] M. Zarka, E. Hay, A. Ostertag, C. Marty, C. Chappard, F. Oudet, et al., Microcracks in subchondral bone plate is linked to less cartilage damage, Bone 123 (2019) 1–7, https://doi.org/10.1016/j.bone.2019.03.011
[14] S. Nakamura, M. Ikebuchi, S. Saeki, D. Furukawa, K. Orita, N. Niimi, et al., Changes in viscoelastic properties of articular cartilage in early stage of osteoarthritis, as determined by optical coherence tomography-based strain rate tomography, BMC Musculoskelet. Disord. 20 (2019) 417, https://doi.org/10.1186/s12891-019-2789-4
[15] N. Fukui, Y. Ikeda, N. Tanaka, The use of laser capture microdissection on adult human articular cartilage for gene expression analysis, Methods Mol. Biol. 755 (2011) 449–459, https://doi.org/10.1007/978-1-61779-163-5_38
[16] T. Scharschmidt, R. Jacquet, J. Laskovski, E. Lowder, S. Weiner, W.J. Landis, Analysis of human osteoarthritic connective tissue by laser capture microdissection and QRT-PCR, Connect Tissue Res. 48 (2007) 316–323, https://doi.org/10.1080/03008200701692685
[17] S. Dube, S. Al-Mannai, L. Liu, S. Tomei, S. Hubrack, S. Sherif, et al., Systematic comparison of quantity and quality of RNA recovered with commercial FFPE tissue extraction kits, J. Transl. Med. 23 (2025) 11, https://doi.org/10.1186/s12967-024-05890-5
[18] D.L. Evers, J. He, Y.H. Kim, J.T. Mason, T.J. O'Leary, Paraffin embedding contributes to RNA aggregation, reduced RNA yield, and low RNA quality, J. Mol. Diagn. 13 (2011) 687–694, https://doi.org/10.1016/j.jmoldx.2011.06.007
[19] B.S. Kowtharapu, C. Marfurt, M. Hovakimyan, F. Will, H. Richter, A. Wree, et al., Femtosecond laser cutting of human corneas for the subbasal nerve plexus evaluation, J. Microsc. 265 (2017) 21–26, https://doi.org/10.1111/jmi.12457
[20] C. Kunert-Keil, H. Richter, I. Zeidler-Rentzsch, I. Bleeker, T. Gredes, Histological comparison between laser microtome sections and ground specimens of implant-containing tissues, Ann. Anat. - Anat. Anz. 222 (2019) 153–157, https://doi.org/10.1016/j.aanat.2018.12.001
[21] F. Wang, Z. Ying, X. Duan, H. Tan, B. Yang, L. Guo, et al., Histomorphometric analysis of adult articular calcified cartilage zone, J. Struct. Biol. 168 (2009) 359–365, https://doi.org/10.1016/j.jsb.2009.08.010
[22] E.B. Hunziker, T.M. Quinn, H.J. Häuselmann, Quantitative structural organization of normal adult human articular cartilage, Osteoarthr. Cartil. 10 (2002) 564–572, https://doi.org/10.1053/joca.2002.0814
[23] P. Omoumi, N. Michoux, E. Thienpont, F.W. Roemer, B.C. Vande Berg, Anatomical distribution of areas of preserved cartilage in advanced femorotibial osteoarthritis using CT arthrography (Part 1), Osteoarthr. Cartil. 23 (2015) 83–87, https://doi.org/10.1016/j.joca.2014.10.006
[24] Siwicki R., Hahaut V., Picelli S. Bulk FLASH-seq V.2 Protocols.io: Berkeley 2023. doi:⟨10.17504/protocols.io.3byl4jynolo5/v2⟩. Available from: ⟨https://www.protocols.io/view/bulk-flash-seq-3byl4jynolo5/v2⟩.
[25] V. Hahaut, D. Pavlinic, W. Carbone, S. Schuierer, P. Balmer, M. Quinodoz, et al., Fast and highly sensitive full-length single-cell RNA sequencing using FLASH-seq, Nat. Biotechnol. 40 (2022) 1447–1451, https://doi.org/10.1038/s41587-022-01312-3
[26] F. Mölder, K.P. Jablonski, B. Letcher, M.B. Hall, C.H. Tomkins-Tinch, V. Sochat, et al., Sustainable data analysis with Snakemake, F1000Res 10 (2021) 33, https://doi.org/10.12688/f1000research.29032.2
[27] M. Martin, Cutadapt removes adapter sequences from high-throughput sequencing reads, EMBnet. J. 17 (2011), https://doi.org/10.14806/ej.17.1.200
[28] A. Dobin, C.A. Davis, F. Schlesinger, J. Drenkow, C. Zaleski, S. Jha, et al., STAR: ultrafast universal RNA-seq aligner, Bioinformatics 29 (2013) 15–21, https://doi.org/10.1093/bioinformatics/bts635
[29] B. Kaminow, D. Yunusov, A. Dobin, STARsolo: accurate, fast and versatile mapping/quantification of single-cell and single-nucleus RNA-seq data (2021), https://doi.org/10.1101/2021.05.05.442755 Available from ⟨https://github.com/alexdobin/STAR/blob/master/docs/STARsolo.md#plate-based-smart-seqscrna-seq⟩.
[30] M. Müller-Gerbl, E. Schulte, R. Putz, The thickness of the calcified layer of articular cartilage: a function of the load supported? J. Anat. 154 (1987) 103–111.
[31] A. Pueyo Moliner, K. Ito, F. Zaucke, D.J. Kelly, M. de Ruijter, J. Malda, Restoring articular cartilage: insights from structure, composition and development, Nat. Rev. Rheumatol. 21 (2025) 291–308, https://doi.org/10.1038/s41584-025-01236-7
[32] G.J.V.M. Van Osch, S.W. Van Der Veen, P. Buma, H.L. Verwoerd-Verhoef, Effect of transforming growth factor-β on proteoglycan synthesis by chondrocytes in relation to differentiation stage and the presence of pericellular matrix, Matrix Biol. 17 (1998) 413–424, https://doi.org/10.1016/S0945-053X(98)90101-9
[33] P. van der Kraan, E. Vitters, W. van den Berg, Differential effect of transforming growth factor beta on freshly isolated and cultured articular chondrocytes, J. Rheumatol. 19 (1992) 140–145.
[34] N.G.M. Thielen, A.P.M. van Caam, V.B. HM, E.L. Vitters, M.H.J. van den Bosch, M.I. Koenders, et al., Separating friend from foe: Inhibition of TGF-β-induced detrimental SMAD1/5/9 phosphorylation while maintaining protective SMAD2/3 signaling in OA chondrocytes, Osteoarthr. Cartil. 31 (2023) 1481–1490, https://doi.org/10.1016/j.joca.2023.08.004
[35] R. Stassen, G.G.H. van den Akker, M.M.J. Caron, D.A.M. Surtel, A. Cremers, L.W. van Rhijn, et al., TGF-β enhances phosphate-driven calcification of human OA articular chondrocytes, Calcif. Tissue Int 116 (2025) 57, https://doi.org/10.1007/s00223-025-01365-x
[36] P.M. van der Kraan, Differential role of transforming growth factor-beta in an osteoarthritic or a healthy joint, J. Bone Metab. 25 (2018) 65–72, https://doi.org/10.11005/jbm.2018.25.2.65
[37] V. Hahaut, S. Picelli, Full-length single-cell RNA-sequencing with FLASH-seq, Methods Mol. Biol. 2584 (2023) 123–164, https://doi.org/10.1007/978-1-0716-2756-3_5
[38] J. Hwang, E.M. Kyubwa, W.C. Bae, W.D. Bugbee, K. Masuda, R.L. Sah, In vitro calcification of immature bovine articular cartilage: formation of a functional zone of calcified cartilage, Cartilage 1 (2010) 287–297, https://doi.org/10.1177/1947603510369552
[39] J. Xu, A. Schwab, E. Salzer, N. Kops, P.A.J. Brama, E. Farrell, et al., Studying the formation of the zone of calcified cartilage in bovine cartilage explants ex vivo, Osteoarthr. Cartil. Open 8 (2026) 100743, https://doi.org/10.1016/j.ocarto.2026.100743
[40] E.E.R. Davis, T.J. Manzoni, V.J. Bianchi, J.F. Weber, P.H. Wu, S.C. Regmi, et al., Passaged articular chondrocytes from the superficial zone and deep zone can regain zone-specific properties after redifferentiation, Am. J. Sports Med. 52 (2024) 1075–1087, https://doi.org/10.1177/03635465241230031
[41] Y. Sun, R. Kandel, Deep zone articular chondrocytes in vitro express genes that show specific changes with mineralization, J. Bone Miner. Res. 14 (1999) 1916–1925, https://doi.org/10.1359/jbmr.1999.14.11.1916
[42] K. von der Mark, T. Kirsch, A. Nerlich, A. Kuss, G. Weseloh, K. Glückert, et al., Type X collagen synthesis in human osteoarthritic cartilage. Indication of chondrocyte hypertrophy, Arthritis Rheum. 35 (1992) 806–811, https://doi.org/10.1002/art.1780350715
[43] T. Kirsch, K. von der Mark, Remodelling of collagen types I, II and X and calcification of human fetal cartilage, Bone Min. 18 (1992) 107–117, https://doi.org/10.1016/0169-6009(92)90851-4
[44] R.L. van Bezooijen, P. ten Dijke, S.E. Papapoulos, C.W. Löwik, SOST/sclerostin, an osteocyte-derived negative regulator of bone formation, Cytokine Growth Factor Rev. 16 (2005) 319–327, https://doi.org/10.1016/j.cytogfr.2005.02.005
[45] R.L. van Bezooijen, B.A. Roelen, A. Visser, L. van der Wee-Pals, E. de Wilt, M. Karperien, et al., Sclerostin is an osteocyte-expressed negative regulator of bone formation, but not a classical BMP antagonist, J. Exp. Med. 199 (2004) 805–814, https://doi.org/10.1084/jem.20031454
[46] R.L. van Bezooijen, S.E. Papapoulos, N.A.T. Hamdy, C.W.G.M. Löwik, Chapter 7 - SOST/Sclerostin: An Osteocyte-Derived Inhibitor of Bone Formation that Antagonizes Canonical Wnt Signaling, in: J.P. Bilezikian, L.G. Raisz, T.J. Martin (Eds.), Principles of Bone Biology, Third Edition, Academic Press, San Diego, 2008, pp. 139–152.
[47] M.M. Weivoda, S.J. Youssef, M.J. Oursler, Sclerostin expression and functions beyond the osteocyte, Bone 96 (2017) 45–50, https://doi.org/10.1016/j.bone.2016.11.024
[48] C. Karlsson, T. Dehne, A. Lindahl, M. Brittberg, A. Pruss, M. Sittinger, et al., Genome-wide expression profiling reveals new candidate genes associated with osteoarthritis, Osteoarthr. Cartil. 18 (2010) 581–592, https://doi.org/10.1016/j.joca.2009.12.002
[49] B.Y. Chan, E.S. Fuller, A.K. Russell, S.M. Smith, M.M. Smith, M.T. Jackson, et al., Increased chondrocyte sclerostin may protect against cartilage degradation in osteoarthritis, Osteoarthr. Cartil. 19 (2011) 874–885, https://doi.org/10.1016/j.joca.2011.04.014
[50] Y. Nossin, E. Farrell, W. Koevoet, F. Datema, R.A. Somoza, A.I. Caplan, et al., The releasate of avascular cartilage demonstrates inherent pro-angiogenic properties in vitro and in vivo, Cartilage 13 (2021) 559s–570s, https://doi.org/10.1177/19476035211047628